Distinguishing Progression from Pseudoprogression in Glioblastoma Using ^{18}F-Fluciclovine PET

Ali Nabavizadeh[1], Stephen J. Bagley[2], Robert K. Doot[1], Jeffrey B. Ware[1], Anthony J. Young[1], Satyam Ghodasara[1], Chao Zhao[3], Hannah Anderson[1], Erin Schubert[1], Erica L. Carpenter[2], Jacob Till[2], Fraser Henderson Jr.[4], Austin R. Pantel[1], H. Isaac Chen[5], John Y.K. Lee[5], Nduka M. Amankulor[2,5], Donald M. O'Rourke[2,5], Arati Desai[2], MacLean P. Nasrallah[6], and Steven Brem[2,5]

[1]*Department of Radiology, Hospital of University of Pennsylvania, Perelman School of Medicine of the University of Pennsylvania, Philadelphia, Pennsylvania;* [2]*Abramson Cancer Center, University of Pennsylvania, Philadelphia, Pennsylvania;* [3]*Department of Surgery, Children's Hospital of Philadelphia, Philadelphia, Pennsylvania;* [4]*Department of Neurosurgery, Loma Linda University Medical Center, Loma Linda, California;* [5]*Department of Neurosurgery, Hospital of University of Pennsylvania, Perelman School of Medicine of the University of Pennsylvania, Philadelphia, Pennsylvania; and* [6]*Division of Neuropathology, Department of Pathology and Laboratory Medicine, Perelman School of Medicine, University of Pennsylvania, Philadelphia, Pennsylvania*

Accurate differentiation between tumor progression (TP) and pseudoprogression remains a critical unmet need in neurooncology. ^{18}F-fluciclovine is a widely available synthetic amino acid PET radiotracer. In this study, we aimed to assess the value of ^{18}F-fluciclovine PET for differentiating pseudoprogression from TP in a prospective cohort of patients with suspected radiographic recurrence of glioblastoma. **Methods:** We enrolled 30 glioblastoma patients with radiographic progression after first-line chemoradiotherapy for whom surgical resection was planned. The patients underwent preoperative ^{18}F-fluciclovine PET and MRI. The relative percentages of viable tumor and therapy-related changes observed in histopathology were quantified and categorized as TP (≥50% viable tumor), mixed TP (<50% and >10% viable tumor), or pseudoprogression (≤10% viable tumor). **Results:** Eighteen patients had TP, 4 had mixed TP, and 8 had pseudoprogression. Patients with TP/mixed TP had a significantly higher 40- to 50-min SUV_{max} (6.64 + 1.88 vs. 4.11 ± 1.52, $P = 0.009$) than patients with pseudoprogression. A 40- to 50-min SUV_{max} cutoff of 4.66 provided 90% sensitivity and 83% specificity for differentiation of TP/mixed TP from pseudoprogression (area under the curve [AUC], 0.86). A maximum relative cerebral blood volume cutoff of 3.672 provided 90% sensitivity and 71% specificity for differentiation of TP/mixed TP from pseudoprogression (AUC, 0.779). Combining a 40- to 50-min SUV_{max} cutoff of 4.66 and a maximum relative cerebral blood volume of 3.67 on MRI provided 100% sensitivity and 80% specificity for differentiating TP/mixed TP from pseudoprogression (AUC, 0.95). **Conclusion:** ^{18}F-fluciclovine PET uptake can accurately differentiate pseudoprogression from TP in glioblastoma, with even greater accuracy when combined with multiparametric MRI. Given the wide availability of ^{18}F-fluciclovine, larger, multicenter studies are warranted to determine whether amino acid PET with ^{18}F-fluciclovine should be used in the routine posttreatment assessment of glioblastoma.

Key Words: MRI; PET; ^{18}F-fluciclovine; glioblastoma; pseudoprogression; tumor progression

J Nucl Med 2023; 64:852–858
DOI: 10.2967/jnumed.122.264812

Received Aug. 21, 2022; revision accepted Dec. 21, 2022.
For correspondence or reprints, contact Ali Nabavizadeh (ali.nabavizadeh@pennmedicine.upenn.edu).
Published online Dec. 22, 2022.

Glioblastoma is the most common malignant primary brain tumor in adults and remains incurable after standard temozolomide-based chemoradiotherapy (*1*). Accurate assessment of tumor response and progression after treatment remains a significant clinical challenge in neurooncology, complicating both routine care and the conduct of clinical trials (*2*). Contrast-enhanced MRI, the current standard for tumor monitoring, lacks specificity for detecting neoplastic progression in the brain. This is largely because an increase in contrast enhancement can be due to any cause of blood–brain barrier breakdown and resultant contrast extravasation, including secondary to effective chemoradiotherapy (*3*). This phenomenon, referred to as pseudoprogression (*4*), has been reported in up to 30% of patients after chemoradiotherapy as defined by the Response Assessment in Neuro-Oncology Working Group (i.e., within 12 wk after completion of radiotherapy) (*5*); however, late pseudoprogression may also occur beyond 12 wk (*6*). Radiographic changes that occur 6 mo to several years after treatment, namely radiation necrosis (*7*), also share common pathophysiologic features with pseudoprogression (*7*).

In posttreatment glioblastoma, accurate differentiation of pseudoprogression from true tumor progression (TP) represents a significant unmet clinical need, as erroneous interpretation can lead to premature discontinuation of an effective treatment or overestimation of the efficacy of subsequent salvage therapies (*8*). In addition, early recognition of TP offers the possibility for earlier therapeutic interventions, such as reresection or recruitment to experimental clinical trials, at a time in the disease course when patients are healthier overall and with relatively preserved performance status. Although advanced MRI techniques such as dynamic susceptibility contrast (DSC), dynamic contrast-enhanced (DCE), and diffusion-weighted imaging have improved the ability to differentiate pseudoprogression from TP, the application of these techniques in both routine practice and clinical trials has been hampered by considerable variability in acquisition and analysis approaches between institutions (*9*). In addition, these techniques have imperfect accuracy and are frequently affected by imaging artifacts, especially in the posttreatment setting (*10*).

Metabolic imaging can provide additional valuable information about tumor status. In particular, PET with amino acid tracers,

including ^{11}C-methionine (*11*), ^{18}F-fluorodopa (*12*), and *O*-(2-^{18}F-fluoroethyl)-L-tyrosine (^{18}F-FET) (*13,14*), have shown value in differentiating pseudoprogression from TP, as amino acid uptake is increased in tumor tissue but low in areas of treatment-related change. Recent expert reviews by the Response Assessment in Neuro-Oncology Working Group found amino acid tracers (^{11}C-methionine, ^{18}F-FET, and ^{18}F-fluorodopa) to have higher diagnostic accuracy than conventional and advanced MRI in the differentiation of glioma recurrence (*15,16*).

^{18}F-fluciclovine is a synthetic amino acid PET tracer approved by the U.S. Food and Drug Administration in the setting of biochemical recurrence of prostate cancer and has an excellent safety profile (*17*). ^{18}F-fluciclovine is an isoleucine analog that is transported into glial cells by both L-amino acid transporters (especially subtype 1) and alanine–serine–cysteine transporters (especially subtype 2), which are upregulated in glioma cells and demonstrate low expression in the normal brain parenchyma (*18*). ^{18}F-fluciclovine has also demonstrated utility for discrimination between low-grade and high-grade glioma (*19–22*). In comparison with ^{11}C-methionine in both treatment-naïve and recurrent glioma, ^{18}F-fluciclovine demonstrated similar detection accuracy but better contrast between tumor and background uptake (*19*). In contrast to ^{11}C-methionine, which has a short half-life (20 min) and is limited to PET centers with a cyclotron (*19*), ^{18}F-fluciclovine has the same longer half-life (109.8 min) as ^{18}F-FET and ^{18}F-fluorodopa, which allows time for it to be shipped from the manufacturer to the imaging centers. In addition, unlike ^{18}F-FET and ^{18}F-fluorodopa, ^{18}F-fluciclovine is widely available in the United States, given its use in the setting of prostate cancer (*23*). Our group previously demonstrated the feasibility of ^{18}F-fluciclovine PET/MRI–guided biopsy in posttreatment glioblastoma to distinguish areas of highest tumor recurrence from areas of treatment-related changes in a small case series (*24*). The aim of this study was to assess the independent and additive value of ^{18}F-fluciclovine PET and multiparametric MRI for differentiating pseudoprogression from TP. Importantly, we used a study cohort in which all patients had available resected tumor tissue to serve as ground truth for TP versus pseudoprogression.

MATERIALS AND METHODS

Study Design and Patient Population

We conducted a prospective cohort study (NCT03990285) of 30 adults with a previously confirmed diagnosis of glioblastoma (defined according to the World Health Organization 2021 classification) (*25*) who were previously treated with standard-of-care radiation and temozolomide and scheduled to have surgery based on radiographic progression (i.e., new contrast-enhancing lesions or lesions showing a ≥25% increase in the sum of the products of the perpendicular diameters on MRI) according to the criteria of the Response Assessment in Neuro-Oncology Working Group (*26*). The patients underwent preoperative multiparametric MRI and 60 min of dynamic brain PET/CT after intravenous administration of ^{18}F-fluciclovine and subsequently underwent maximal safe resection of the enhancing lesion. The percentages of viable tumor and therapy-related changes comprising the specimen were quantified on histopathology by a board-certified neuropathologist. All patients provided written informed consent. This study was approved by the Institutional Review Board of the University of Pennsylvania.

Image Acquisition

PET. ^{18}F-fluciclovine (Axumin; Blue Earth Diagnostics) was produced by PETNET Solutions facilities under U.S. Pharmacopeia–compliant procedures and was administered under an investigational-new-drug application exemption. All PET studies were performed on an Ingenuity TF PET/CT device (Philips Healthcare) using a previously described method of image reconstruction (*27*). Patients underwent 60 min of dynamic PET imaging after injection of 191 ± 21 MBq of ^{18}F-fluciclovine. In 2 patients, PET acquisition was performed for 40 and 45 min instead of 60 min. Patients fasted for 4 h before administration of ^{18}F-fluciclovine. The patients were monitored for adverse events for 24 h after each injection of the ^{18}F-fluciclovine radiotracer, and none were observed.

MRI. Brain MRI was performed using the brain tumor imaging protocol of the University of Pennsylvania on a 3-T magnet (Trio; Siemens), which included an axial T1-weighted 3-dimensional magnetization-prepared rapid gradient echo sequence before and after contrast administration, a postcontrast axial fluid-attenuated inversion recovery sequence, a diffusion tensor imaging sequence ($n = 30$), a DCE perfusion sequence ($n = 29$), and a DSC perfusion sequence ($n = 27$ after excluding 2 patients with degraded source data due to susceptibility effects). Representative imaging parameters are presented in Supplemental Table 1 (supplemental materials are available at http://jnm.snmjournals.org). Two contrast boluses (gadoterate meglumine; Guerbet) with a dose of 0.1 mmol/kg were sequentially administered for DCE followed by DSC imaging, with the dose administered for DCE serving as a preload dose for DSC to reduce the effect of contrast agent leakage on relative cerebral blood volume (rCBV) measurements.

Image Analysis

PET. PET measurements were performed in MIM (the versions were updated throughout the study from 6.9 to 7.1). Volumes of interest were defined in the resected tumor using PET images and coregistered to T1 postcontrast MR images and fluid-attenuated inversion recovery images, with placement confirmed by a board-certified neuroradiologist and a nuclear radiologist. Measurements were taken of tumor SUV_{max}, 1 cm^3 SUV_{peak}, and 50% threshold SUV_{mean} defined on summed images at 20–30, 30–40, 40–50, 50–60, 40–60, and 30–60 min after injection (g/mL units). Normal-tissue volumes of interest and SUV_{mean} measurements were made in the contralateral normal brain, pituitary gland, and superior sagittal sinus. The volumes of interest in the contralateral normal brain were 20 mm in diameter, whereas those in the pituitary and superior sagittal sinus were 15 mm in diameter. Tumor SUVs and SUV ratios normalized to each normal-tissue SUV_{mean} were calculated.

Time–activity curves of ^{18}F-fluciclovine SUV_{peak} uptake in the tumor were generated by application, to the entire dynamic dataset, of a spheric volume of interest with a volume of 1 cm^3 centered on maximal tumor uptake. Time–activity curves for each lesion were visually assessed by an experienced board-certified nuclear radiologist as previously described (*28*) and assigned to one of the following curve patterns: constantly increasing without identifiable peak uptake (pattern I), peaking at a midpoint followed by a plateau or a small descent (pattern II), and peaking early followed by a constant descent (pattern III) (*28*). In addition, time to peak (TTP) with a lower threshold time of at least 10 min was measured and compared among groups.

MRI. Regions of abnormal contrast enhancement, necrosis, and nonenhancing fluid-attenuated inversion recovery signal intensity were segmented using a semiautomated segmentation tool (ITK-SNAP) (*29*) followed by manual editing by 2 board-certified neuroradiologists. Diffusion tensor imaging was processed with FSL (*30*) and included removal of nonbrain tissue as well as correction for motion and eddy currents. Diffusion data were then fit to the tensor model, and maps of whole-brain apparent diffusion coefficients were used in subsequent analysis.

DCE images were corrected for motion, and nonbrain tissue was removed using image processing tools available in FSL. DCE data were then analyzed using the extended Toft model, as implemented by

the ROCKETSHIP software package (*31*) in the MATLAB programming environment (2014a; MathWorks), to derive voxelwise maps of the volume transfer constant Ktrans, plasma volume fraction Vp, extravascular extracellular volume fraction Ve, and washout rate constant of contrast agent from the EES to the intravascular space Kep defined as Kep = Ktrans/Ve. Because of the inconsistent availability of T1 mapping among subjects, a fixed prebolus T1 value (1,000 ms) was used to transform signal intensity curves to contrast concentration curves in DCE analysis. DSC data were used to generate leakage-corrected rCBV maps using the γ-variate function as implemented in NordicICE software (NordicNeuroLab). For each functional modality (diffusion tensor imaging, DCE, and DSC), a reference image derived from source data was used to compute a linear transformation from the functional space to the subject's T1 postcontrast magnetization-prepared rapid gradient echo sequence using the Advanced Normalization Tools registration tool (*32*). These transformations were then used to coregister all parameter maps to the anatomic space. DCE and DSC imaging metrics were normalized to the median value of a region of interest placed in normal-appearing white matter by a board-certified neuroradiologist at the same slice levels as the abnormality. Subsequent statistical analysis was based on the mean rCBV and maximum rCBV ($rCBV_{max}$) and DCE metric values as well as the mean and minimum apparent diffusion coefficients extracted from the intersection of the segmented contrast-enhanced and PET ROI.

Histopathologic Evaluation and Analysis of Molecular Markers

After resection, the surgically extracted tissue specimens were entirely fixed in 10% buffered formalin, routinely processed, and embedded in paraffin. Five-micrometer-thick sections of each specimen were cut onto glass slides, stained with hematoxylin and eosin, and assessed by a board-certified neuropathologist (who was unaware of the preoperative MRI and PET imaging data). The presence or absence of pseudopalisading necrosis and microvascular proliferation (features of recurrent glioblastoma), the presence or absence of dystrophic calcification and vascular hyalinization, and the percentage of geographic necrosis (representative of treatment-related changes) were quantified. Proliferative activity was determined by quantification of the number of mitotic figures in 10 high-power fields and semiquantitative assessment of the Ki-67 proliferative index by immunostaining (mouse monoclonal, MIB-1, IR62661; Dako). On the basis of the combined assessment of these features, the entire resected specimen was assigned a tumor percentage of 0%–100%. Patients were considered TP if viable tumor represented at least 50% of the resected specimen, mixed TP if less than 50% and more than 10%, and pseudoprogression if no more than 10%.

Statistical Methods

Given that the number of PET variables (6 summed images and normalized to normal contralateral brain, pituitary, and superior sagittal sinus) and MRI variables was higher than the number of subjects, the least absolute shrinkage and selection operator (LASSO) was used to determine the variables most predictive of viable tumor percentage on histopathology. In addition to imaging variables, the clinical variables of age, sex, *O*-6-methylguanine methyltransferase (*MGMT*) promoter methylation status, and duration from the end of first-line radiotherapy to recurrent surgery were included in the LASSO analysis. The strengths of correlations between primary outcome and selected variables were assessed by Pearson correlation or point-biserial correlation (rpb). A receiver-operating-characteristic curve was used to illustrate the diagnostic ability of a binary classifier system as its discrimination threshold was varied. The criteria for determination of the most appropriate cutoff was based on the point on the curve at a minimum distance from the left upper corner of the unit square. Furthermore, the leave-one-out cross-validation procedure was used to estimate the performance of the LASSO regression model by making predictions on test data. The differences in PET uptake between different groups (TP/mixed TP vs. pseudoprogression and TP vs. pseudoprogression) were compared using the Wilcoxon rank-sum exact test. The Kruskal–Wallis test was used to compare time to peak (TTP) between different groups. The χ^2 test was performed to compare MGMT methylation status in patients with TP compared with pseudoprogression. An α value of 0.05 was used as the cutoff for significance. All the statistical analyses were computed using code written in R, version 4.1.0 (R Foundation).

RESULTS

The baseline characteristics of the study cohort are summarized in Table 1. Histopathologic analysis revealed 18 patients with TP, 4 with mixed TP, and 8 with pseudoprogression. Tumor percentage ranged from 0% to 100% (median, 57.50%; SD, 31.66), and Ki-67 ranged from 1% to 70% (median, 10%; SD, 13.38). Of patients with TP, 8 of 18 (44%) had MGMT methylated tumors. Of patients with pseudoprogression, 1 of 8 (13%) had MGMT methylated tumor. A χ^2 test revealed no statistically significant difference in the rate of MGMT methylation between patients with TP and those with pseudoprogression ($P = 0.29$). All patients in this study (100%) had isocitrate dehydrogenase wild-type tumors. A detailed description of demographics, clinical symptoms at the time of radiographic progression, MGMT and isocitrate dehydrogenase status, and tumor percentage on histopathology is provided in Supplemental Table 2).

Correlation of ^{18}F-Fluciclovine PET and MRI Parameters with Histopathologic and Clinical Variables

A 50- to 60-min 50% threshold SUV_{mean} ($r = 0.54$, $P = 0.004$), 50- to 60-min 50% threshold SUV_{mean}/superior sagittal sinus

TABLE 1
Demographics and Baseline Clinical Characteristics of Patients (n = 30)

Characteristic	Data
Sex	
Male	10 (33.3)
Female	20 (66.7)
Age (y)	62 (31–81)
MGMT status	
Positive (methylated)	10 (33.3)
Negative (unmethylated)	19 (63.3)
Unknown	1 (3.3)
Dose of first-line radiotherapy received (Gy)	
40	6 (20)
60	22 (73.3)
75	2 (6.7)
Interval between completion of radiotherapy and surgery for recurrent glioblastoma (wk)	31.7 (5–283)
Interval between PET scan and surgery for recurrent glioblastoma (d)	4 (1–13)

Qualitative data are number and percentage; continuous data are median and range.

TABLE 2
Analysis of PET and MRI Parameters for Differentiation of TP/Mixed TP from Pseudoprogression

Variable	OR	rpb	*P*
40- to 50-min SUV_{max}	1.14	0.49	0.011
40- to 50-min SUV_{max}/pituitary	1.43	0.56	0.003
$rCBV_{max}$	1.13	0.47	0.016

($r = 0.55$, $P = 0.003$), and a 40- to 50-min SUV_{max}/pituitary ($r = 0.51$, $P = 0.008$) correlated positively with viable tumor percentage on histopathology. Among the MRI parameters, only $rCBV_{max}$ was selected by the LASSO analysis and had a positive correlation with tumor percentage ($r = 0.49$; $P = 0.011$). The 40- to 50-min SUV_{peak} correlated positively with Ki-67 ($r = 0.38$), with a trend toward significance ($P = 0.056$). There was no correlation between tumor percentage and age, sex, *MGMT* promoter methylation status, time elapsed between end of radiation and the patient's reoperation, or prior radiotherapy dose.

Differentiation of TP/Mixed TP from Pseudoprogression

Analysis of 25 subjects who had all the PET and MRI parameters (Table 2) demonstrated that patients with histopathologically proven TP/mixed TP had a higher 40- to 50-min SUV_{max} (odds ratio [OR], 1.14; rpb, 0.49; $P = 0.011$) and 40- to 50-min SUV_{max}/pituitary (OR, 1.43; rpb, 0.56; $P = 0.003$). None of the PET variables normalized to normal brain were selected by the LASSO analysis. Among the MRI parameters, $rCBV_{max}$ (OR, 1.13; rpb, 0.47, $P = 0.016$) was higher in the TP/mixed TP groups than in the pseudoprogression group. Other MRI parameters were not selected by the LASSO analysis.

Analysis of 28 subjects with an available 0- to 60-min dynamic acquisition demonstrated that the 50- to 60-min 50% threshold SUV_{mean} (OR, 1.31; rpb, 0.52, $P = 0.004$), 40- to 50-min SUV_{max} (OR, 1.20; rpb, 0.50, $P = 0.005$), 40- to 50-min SUV_{max}/pituitary (OR, 1.01; rpb, 0.47, $P = 0.010$), and 20- to 30-min SUV_{max} (OR, 1.12; rpb, 0.49, $P = 0.007$) were higher in the TP/mixed TP group than in the pseudoprogression group.

Patients who demonstrated TP/mixed TP had a significantly higher 40- to 50-min SUV_{max} (6.64 ± 1.88 vs. 4.11 ± 1.52, $P = 0.009$) and 20- to 30-min SUV_{max} (6.59 ± 2.15 vs. 3.89 ± 1.30, $P = 0.002$) than did patients with histologic pseudoprogression (Fig. 1). An illustrative case in which ^{18}F-fluciclovine PET uptake correctly predicted TP, whereas rCBV on DSC perfusion MRI did not, is displayed in Figure 2.

Although the main purpose of this work was to differentiate patients with TP/mixed TP from those with pseudoprogression, an exploratory analysis was also performed to differentiate TP from pseudoprogression (Supplemental Results; Supplemental Fig. 1; Supplemental Table 3).

Receiver-Operating-Characteristic Curve Analyses

A 20- to 30-min SUV_{max} cutoff of 4.457 provided 95% sensitivity and 83% specificity for differentiation of TP/mixed TP from pseudoprogression (area under the curve [AUC], 0.902). A 40- to 50-min SUV_{max} cutoff of 4.662 provided 90% sensitivity and 83% specificity for differentiation of TP/mixed TP from pseudoprogression (AUC, 0.856). An $rCBV_{max}$ cutoff of 3.672 provided 90% sensitivity and 71% specificity for differentiation of TP/mixed TP from pseudoprogression (AUC, 0.779). Combining a 40- to 50-min SUV_{max} cutoff of 4.662 and an $rCBV_{max}$ cutoff of 3.672 provided 100% sensitivity and 80% specificity for differentiating TP/mixed TP from pseudoprogression (AUC, 0.95; Fig. 3). A similar AUC of 0.95 was obtained after combining a 20- to 30-min SUV_{max} cutoff of 4.457 and an $rCBV_{max}$ cutoff of 3.672. Combining a 40- to 50-min SUV_{max} cutoff of 4.662 and an $rCBV_{max}$ cutoff of 3.672

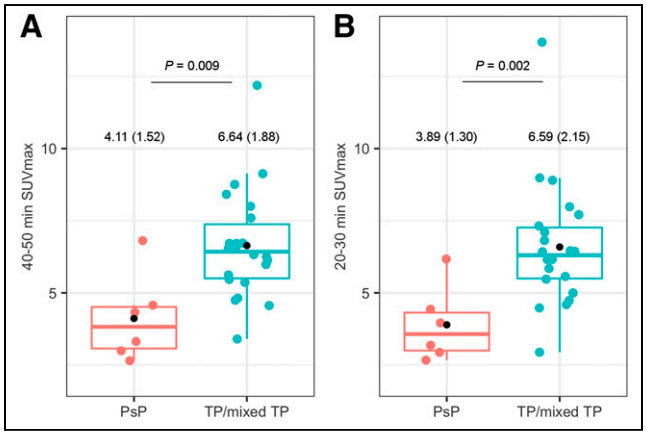

FIGURE 1. Comparison of PET parameters in patients with TP/mixed TP vs. pseudoprogression. PsP = pseudoprogression.

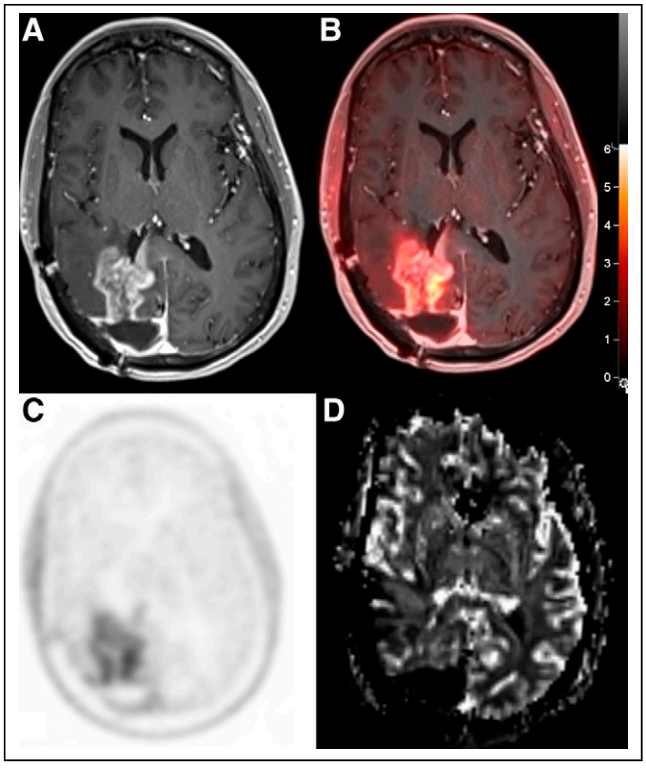

FIGURE 2. Example of false-negative MRI results. In postcontrast T1 (A) and fused PET/MRI (B), a 65-y-old man with history of right occipital glioblastoma showed progressive enhancement adjacent to resection cavity. (C and D) ^{18}F-fluciclovine PET imaging (C) demonstrated marked increased uptake (SUV_{max}, 5.46) compared with only mild increase (rCBV, 2.43) in $rCBV_{map}$ on DSC perfusion MRI (D). Patient underwent resection, and pathology showed that 60% of specimen consisted of viable tumor and 40% consisted of therapy-related changes. The intensity scale bar represents SUV.

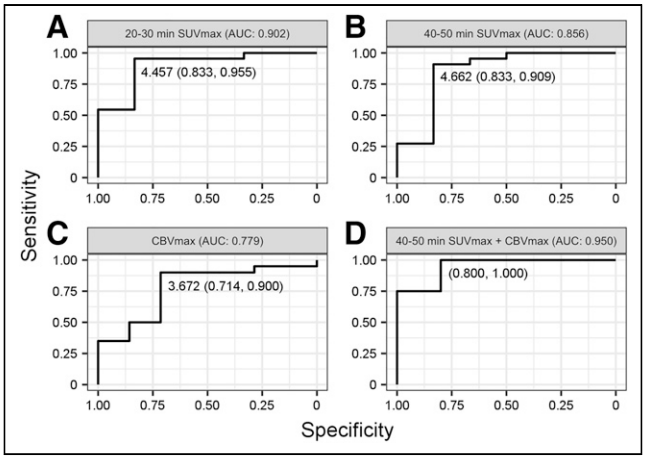

FIGURE 3. Receiver-operating-characteristic curve analysis of 20- to 30-min SUV_{max} (A), 40- to 50-min SUV_{max} (B), $rCBV_{max}$ (C), and combined 40- to 50-min SUV_{max}–$rCBV_{max}$ (D) to differentiate TP/mixed TP from pseudoprogression.

applying leave-one-out cross-validation provided 100% sensitivity and 80% specificity for differentiation of TP/mixed TP from pseudoprogression (AUC, 0.800; Supplemental Fig. 2).

PET Tracer Kinetics

The time–activity curve demonstrated accumulation at the tumor bed that reached a steady state after 20 min (Fig. 4A). All patients except two demonstrated a type II (plateau) pattern (Fig. 4B). One patient with TP and extracranial extension of tumor to the overlying scalp demonstrated a type III pattern. One patient with TP demonstrated a type I pattern. The TTP did not differ ($P = 0.830$) between groups (Fig. 4C). Representative patients from the TP, TP/mixed TP, and pseudoprogression groups are demonstrated in Figure 5.

DISCUSSION

In this study, we demonstrated that ^{18}F-fluciclovine PET can accurately differentiate pseudoprogression from TP/mixed TP in glioblastoma patients after chemoradiotherapy. The accuracy of ^{18}F-fluciclovine PET in our study is in the higher range of prior studies using ^{18}F-FET and ^{18}F-fluorodopa and higher than with ^{11}C-methionine PET (*13,14,16,28,33–41*). In addition, we demonstrated that ^{18}F-fluciclovine PET has higher accuracy than advanced MRI sequences and that combining ^{18}F-fluciclovine PET with DSC perfusion MRI resulted in even better performance for differentiation between TP/mixed TP and pseudoprogression. A recent study of 21 patients with suspected recurrent high-grade glioma who received ^{18}F-fluciclovine PET imaging (*42*) demonstrated a high median lesion-to-background ratio (*42*); however, no patients with confirmed pseudoprogression were included. To the best of our knowledge, our study is the first report that demonstrates the ability of ^{18}F-fluciclovine PET to discriminate between TP and pseudoprogression. We also found a positive correlation between Ki-67 and PET parameters, which is consistent with a previous ^{18}F-fluciclovine study on biopsy-proven low- and high-grade gliomas (*20*) and a report of ^{18}F-fluciclovine PET/MRI–guided biopsy in a patient with treatment-naïve oligodendroglioma (*21*).

Although multiparametric MRI including postcontrast imaging is widely used for posttreatment surveillance of glioblastoma, differentiation of pseudoprogression from TP using MRI is challenging because both of these entities may disrupt the blood–brain barrier and lead to contrast extravasation and enhancement (*43*). Amino acid PET imaging enables analysis of the tumor environment beyond disruption of the blood–brain barrier because it is based on upregulation of amino acid transporters in the tumor cells (independent of blood–brain barrier disruption) (*44–46*). In addition, chronic blood products in the surgical bed cause susceptibility artifacts and interfere with advanced MRI techniques such as DSC perfusion imaging, frequently confounding studies in posttreatment glioblastoma patients. In our study, DSC perfusion images were nondiagnostic in 2 patients and had to be excluded. Multiple studies compared the diagnostic accuracy of ^{18}F-FET PET and DSC perfusion MRI, and the results ranged from superior performance for PET to equal performance for both modalities (*34,47–49*). PET and DSC perfusion imaging were found to have added value in some studies (*34,48,49*), but these consisted of heterogeneous cohorts with grades 2–4 glioma, and the final diagnosis was based on histology in only a subset of patients. Our results showed that the accuracy of DSC MRI was comparable to that observed in prior studies, and multiparametric analysis of PET and MRI provided improved accuracy in our study, consistent with prior ^{18}F-FET studies (*34,47,49*).

Unlike other amino acid PET agents, we found that absolute SUV measurements are more accurate for differentiating pseudoprogression from TP than are normalized tumor-to-brain ratios, secondary to very low normal-brain uptake and variability of normal-brain uptake between patients. Conversely, normalization of SUV_{max} to the pituitary gland showed similar accuracy to SUV_{max} in differentiation of TP/mixed TP from pseudoprogression. Previous studies with ^{18}F-FET demonstrated the usefulness of a time–activity curve with curve pattern II or III and a TTP of less than 45 min for differentiating TP from treatment-related changes (*34,35,50*). In our study, we did not find TTP and time–activity curve patterns to be useful because almost all patients demonstrated a type II (plateau) pattern, consistent with a prior study on pretreatment glioma (*17*). One patient with extracranial extension of tumor to the overlying scalp demonstrated a type III pattern (uptake peaking early followed by a constant descent), similar to the described literature on prostate cancer (*51*).

Our study had limitations, including its single-institution nature, which warrants future multicenter prospective studies to

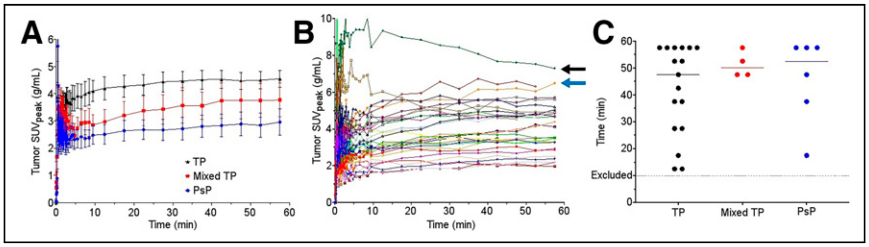

FIGURE 4. (A) Comparison of mean time–activity curves in patients with TP, mixed TP, and pseudoprogression demonstrated accumulation at tumor bed that reached steady state after 20 min. (B) Time–activity curves in individual patients. All patients except two demonstrated type II (plateau) pattern. One patient with TP and extracranial extension of tumor (black arrow) to overlying scalp demonstrated type III pattern, and 1 patient with TP demonstrated type I pattern (blue arrow). (C) Comparison of mean TTP in patients with TP, mixed TP, and pseudoprogression. PsP = pseudoprogression.

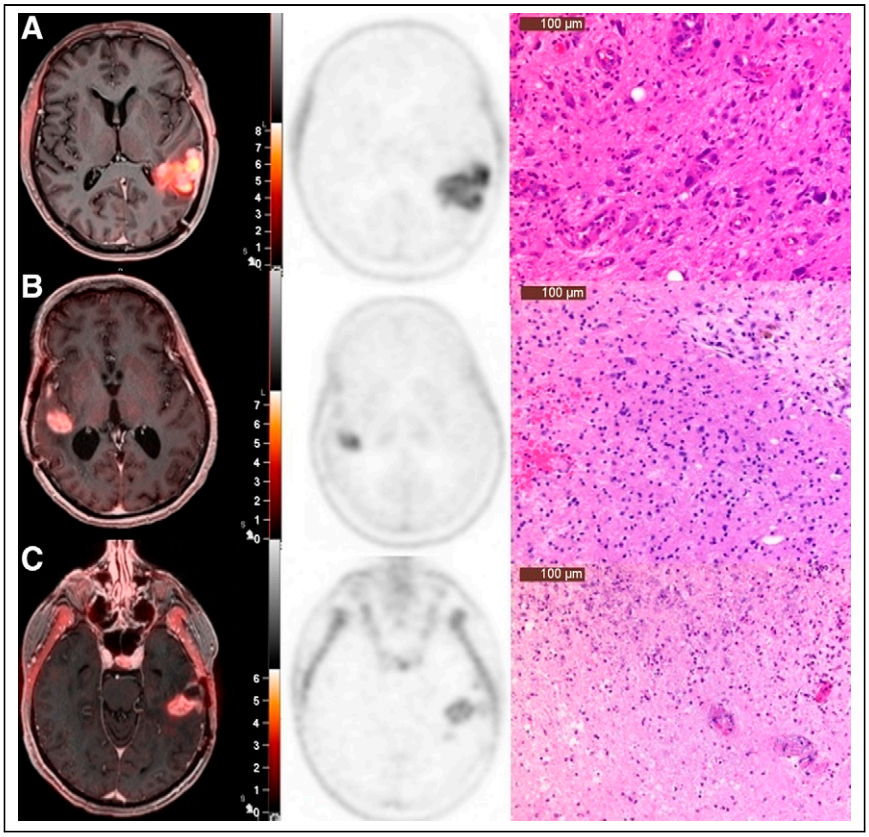

FIGURE 5. Imaging and histopathologic findings in 3 patients with true progression (A), mixed true progression–pseudoprogression (B), and pseudoprogression (C). (A) A 69-y-old woman with history of left temporoparietal glioblastoma with progressive enhancement in resection bed. ^{18}F-fluciclovine PET imaging demonstrated marked increased uptake (SUV_{max}, 6.73). Patient underwent resection, and histopathology showed that most resected tissue comprised atypical glial cells, with enlarged, irregular, hyperchromatic nuclei consistent with recurrent glioma (overall, 80% tumor). (B) A 64-y-old woman with history of right temporal glioblastoma with progressive enhancement in resection bed. ^{18}F-fluciclovine PET imaging demonstrated moderate increased uptake (SUV_{max}, 4.75). Histopathology demonstrated treatment-related changes and 40% infiltrating glioma throughout specimen. (C) A 65-y-old man with history of left temporal glioblastoma with progressive enhancement in resection bed. ^{18}F-fluciclovine PET imaging demonstrated only mild uptake (SUV_{max}, 2.65). Histopathology demonstrated abundant treatment-related changes with no tumor in specimen. The intensity scale bar represents SUV.

validate the generalizability of our findings. However, the prospective design, availability of histopathologic confirmation for all patients, and short interval between ^{18}F-fluciclovine PET and surgery are unique strengths compared with most prior studies of amino acid PET tracers, which have been largely retrospective and have relied on clinical follow-up to distinguish TP from pseudoprogression in most patients. In this study, all patients underwent dynamic PET imaging over 60 min. Given the 20-min plateau in uptake and the high accuracy of both 20- to 30-min and 40- to 50-min SUV_{max}, static imaging with both these imaging windows can be used in clinical practice, depending on the preference of the center. Given the significant uptake when compared with normal brain parenchyma in all patients (Fig. 5), quantitative criteria and not visual analysis alone is needed to differentiate between TP and pseudoprogression. Overall, our results suggest that ^{18}F-fluciclovine PET imaging can accurately differentiate pseudoprogression from TP in glioblastoma patients. Given the wide availability of ^{18}F-fluciclovine, studies that are larger and multicenter are warranted to determine whether amino acid PET imaging with ^{18}F-fluciclovine should be used in the routine posttreatment assessment of glioblastoma.

CONCLUSION

^{18}F-fluciclovine PET uptake can accurately differentiate pseudoprogression from TP in glioblastoma, with even greater accuracy when combined with multiparametric MRI. Given the wide availability of ^{18}F-fluciclovine, larger, multicenter studies are warranted to determine whether amino acid PET with ^{18}F-fluciclovine should be used in the routine posttreatment assessment of glioblastoma.

DISCLOSURE

Ali Nabavizadeh received research funding (paid to the institution) from Blue Earth Diagnostics and compensation of travel expenses to present the results of this study. No other potential conflict of interest relevant to this article was reported.

KEY POINTS

QUESTION: Can ^{18}F-fluciclovine PET distinguish progression from pseudoprogression in glioblastoma?

PERTINENT FINDINGS: Our prospective study demonstrated that ^{18}F-fluciclovine PET uptake correlated with tumor percentage on histology and can distinguish progression from pseudoprogression in glioblastoma.

IMPLICATIONS FOR PATIENT CARE: Given the wide availability of ^{18}F-fluciclovine in the United States as a Food and Drug Administration–approved radiotracer, this study has immediate translational relevance.

REFERENCES

1. Stupp R, Mason WP, van den Bent MJ, et al. Radiotherapy plus concomitant and adjuvant temozolomide for glioblastoma. *N Engl J Med.* 2005;352:987–996.
2. Ellingson BM, Wen PY, Cloughesy TF. Modified criteria for radiographic response assessment in glioblastoma clinical trials. *Neurotherapeutics.* 2017;14:307–320.
3. Hygino da Cruz LC Jr, Rodriguez I, Domingues RC, Gasparetto EL, Sorensen AG. Pseudoprogression and pseudoresponse: imaging challenges in the assessment of posttreatment glioma. *AJNR.* 2011;32:1978–1985.
4. Langen KJ, Galldiks N, Hattingen E, Shah NJ. Advances in neuro-oncology imaging. *Nat Rev Neurol.* 2017;13:279–289.
5. Wen PY, Chang SM, Van den Bent MJ, Vogelbaum MA, Macdonald DR, Lee EQ. Response assessment in neuro-oncology clinical trials. *J Clin Oncol.* 2017;35:2439–2449.
6. Kebir S, Fimmers R, Galldiks N, et al. Late pseudoprogression in glioblastoma: diagnostic value of dynamic O-(2-[^{18}F]fluoroethyl)-L-tyrosine PET. *Clin Cancer Res.* 2016;22:2190–2196.
7. Ellingson BM, Chung C, Pope WB, Boxerman JL, Kaufmann TJ. Pseudoprogression, radionecrosis, inflammation or true tumor progression? Challenges associated with glioblastoma response assessment in an evolving therapeutic landscape. *J Neurooncol.* 2017;134:495–504.
8. Reardon DA, Weller M. Pseudoprogression: fact or wishful thinking in neuro-oncology? *Lancet Oncol.* 2018;19:1561–1563.

9. Patel P, Baradaran H, Delgado D, et al. MR perfusion-weighted imaging in the evaluation of high-grade gliomas after treatment: a systematic review and meta-analysis. *Neuro-oncol.* 2017;19:118–127.
10. van Dijken BRJ, van Laar PJ, Smits M, Dankbaar JW, Enting RH, van der Hoorn A. Perfusion MRI in treatment evaluation of glioblastomas: clinical relevance of current and future techniques. *J Magn Reson Imaging.* 2019;49:11–22.
11. Terakawa Y, Tsuyuguchi N, Iwai Y, et al. Diagnostic accuracy of ^{11}C-methionine PET for differentiation of recurrent brain tumors from radiation necrosis after radiotherapy. *J Nucl Med.* 2008;49:694–699.
12. Chen W, Silverman DH, Delaloye S, et al. ^{18}F-FDOPA PET imaging of brain tumors: comparison study with ^{18}F-FDG PET and evaluation of diagnostic accuracy. *J Nucl Med.* 2006;47:904–911.
13. Pöpperl G, Götz C, Rachinger W, Gildehaus FJ, Tonn JC, Tatsch K. Value of O-(2-[^{18}F]fluoroethyl)-L-tyrosine PET for the diagnosis of recurrent glioma. *Eur J Nucl Med Mol Imaging.* 2004;31:1464–1470.
14. Rachinger W, Goetz C, Pöpperl G, et al. Positron emission tomography with O-(2-[^{18}F]fluoroethyl)-L-tyrosine versus magnetic resonance imaging in the diagnosis of recurrent gliomas. *Neurosurgery.* 2005;57:505–511.
15. Albert NL, Weller M, Suchorska B, et al. Response Assessment in Neuro-Oncology Working Group and European Association for Neuro-Oncology recommendations for the clinical use of PET imaging in gliomas. *Neuro Oncol.* 2016;18:1199–1208.
16. Galldiks N, Niyazi M, Grosu AL, et al. Contribution of PET imaging to radiotherapy planning and monitoring in glioma patients: a report of the PET/RANO group. *Neuro Oncol.* 2021;23:881–893.
17. Kondo A, Ishii H, Aoki S, et al. Phase IIA clinical study of [^{18}F]fluciclovine: efficacy and safety of a new PET tracer for brain tumors. *Ann Nucl Med.* 2016;30:608–618.
18. Shoup TM, Olson J, Hoffman JM, et al. Synthesis and evaluation of [^{18}F]1-amino-3-fluorocyclobutane-1-carboxylic acid to image brain tumors. *J Nucl Med.* 1999;40:331–338.
19. Michaud L, Beattie BJ, Akhurst T, et al. ^{18}F-fluciclovine (^{18}F-FACBC) PET imaging of recurrent brain tumors. *Eur J Nucl Med Mol Imaging.* 2020;47:1353–1367.
20. Parent EE, Benayoun M, Ibeanu I, et al. [^{18}F]fluciclovine PET discrimination between high- and low-grade gliomas. *EJNMMI Res.* 2018;8:67.
21. Karlberg A, Berntsen EM, Johansen H, et al. Multimodal ^{18}F-fluciclovine PET/MRI and ultrasound-guided neurosurgery of an anaplastic oligodendroglioma. *World Neurosurg.* 2017;108:989.e1–989.e8.
22. Wakabayashi T, Iuchi T, Tsuyuguchi N, et al. Diagnostic performance and safety of positron emission tomography using ^{18}F-fluciclovine in patients with clinically suspected high- or low-grade gliomas: a multicenter phase IIB trial. *Asia Ocean J Nucl Med Biol.* 2017;5:10–21.
23. Songmen S, Nepal P, Olsavsky T, Sapire J. Axumin positron emission tomography: novel agent for prostate cancer biochemical recurrence. *J Clin Imaging Sci.* 2019;9:49.
24. Henderson F Jr, Brem S, O'Rourke DM, et al. ^{18}F-fluciclovine PET to distinguish treatment-related effects from disease progression in recurrent glioblastoma: PET fusion with MRI guides neurosurgical sampling. *Neurooncol Pract.* 2020;7:152–157.
25. Louis DN, Perry A, Wesseling P, et al. The 2021 WHO classification of tumors of the central nervous system: a summary. *Neuro Oncol.* 2021;23:1231–1251.
26. Wen PY, Macdonald DR, Reardon DA, et al. Updated response assessment criteria for high-grade gliomas: Response Assessment in Neuro-Oncology Working Group. *J Clin Oncol.* 2010;28:1963–1972.
27. Kolthammer JA, Su KH, Grover A, Narayanan M, Jordan DW, Muzic RF. Performance evaluation of the ingenuity TF PET/CT scanner with a focus on high count-rate conditions. *Phys Med Biol.* 2014;59:3843–3859.
28. Galldiks N, Dunkl V, Stoffels G, et al. Diagnosis of pseudoprogression in patients with glioblastoma using O-(2-[^{18}F]fluoroethyl)-L-tyrosine PET. *Eur J Nucl Med Mol Imaging.* 2015;42:685–695.
29. Yushkevich PA, Piven J, Hazlett HC, et al. User-guided 3D active contour segmentation of anatomical structures: significantly improved efficiency and reliability. *Neuroimage.* 2006;31:1116–1128.
30. Smith SM, Jenkinson M, Woolrich MW, et al. Advances in functional and structural MR image analysis and implementation as FSL. *Neuroimage.* 2004;23(suppl 1):S208–S219.
31. Barnes SR, Ng TS, Santa-Maria N, Montagne A, Zlokovic BV, Jacobs RE. Rocketship: a flexible and modular software tool for the planning, processing and analysis of dynamic MRI studies. *BMC Med Imaging.* 2015;15:19.
32. Avants BB, Epstein CL, Grossman M, Gee JC. Symmetric diffeomorphic image registration with cross-correlation: evaluating automated labeling of elderly and neurodegenerative brain. *Med Image Anal.* 2008;12:26–41.
33. Mihovilovic MI, Kertels O, Hänscheid H, et al. O-(2-(^{18}F)fluoroethyl)-L-tyrosine pet for the differentiation of tumour recurrence from late pseudoprogression in glioblastoma. *J Neurol Neurosurg Psychiatry.* 2019;90:238–239.
34. Pyka T, Hiob D, Preibisch C, et al. Diagnosis of glioma recurrence using multiparametric dynamic ^{18}F-fluoroethyl-tyrosine PET-MRI. *Eur J Radiol.* 2018;103:32–37.
35. Galldiks N, Stoffels G, Filss C, et al. The use of dynamic O-(2-^{18}F-fluoroethyl)-L-tyrosine PET in the diagnosis of patients with progressive and recurrent glioma. *Neuro Oncol.* 2015;17:1293–1300.
36. Karunanithi S, Sharma P, Kumar A, et al. ^{18}F-FDOPA PET/CT for detection of recurrence in patients with glioma: prospective comparison with ^{18}F-FDG PET/CT. *Eur J Nucl Med Mol Imaging.* 2013;40:1025–1035.
37. Minamimoto R, Saginoya T, Kondo C, et al. Differentiation of brain tumor recurrence from post-radiotherapy necrosis with ^{11}C-methionine PET: visual assessment versus quantitative assessment. *PLoS One.* 2015;10:e0132515.
38. Nihashi T, Dahabreh IJ, Terasawa T. Diagnostic accuracy of PET for recurrent glioma diagnosis: a meta-analysis. *AJNR.* 2013;34:944–950.
39. Karunanithi S, Sharma P, Kumar A, et al. Comparative diagnostic accuracy of contrast-enhanced MRI and ^{18}F-FDOPA PET-CT in recurrent glioma. *Eur Radiol.* 2013;23:2628–2635.
40. Werner JM, Weller J, Ceccon G, et al. Diagnosis of pseudoprogression following lomustine-temozolomide chemoradiation in newly diagnosed glioblastoma patients using FET-PET. *Clin Cancer Res.* 2021;27:3704–3713.
41. Salber D, Stoffels G, Pauleit D, et al. Differential uptake of O-(2-^{18}F-fluoroethyl)-L-tyrosine, L-3H-methionine, and 3H-deoxyglucose in brain abscesses. *J Nucl Med.* 2007;48:2056–2062.
42. Bogsrud TV, Londalen A, Brandal P, et al. ^{18}F-fluciclovine PET/CT in suspected residual or recurrent high-grade glioma. *Clin Nucl Med.* 2019;44:605–611.
43. Bagley SJ, Schwab RD, Nelson E, et al. Histopathologic quantification of viable tumor versus treatment effect in surgically resected recurrent glioblastoma. *J Neurooncol.* 2019;141:421–429.
44. Ono M, Oka S, Okudaira H, et al. Comparative evaluation of transport mechanisms of trans-1-amino-3-[^{18}F]fluorocyclobutanecarboxylic acid and l-[methyl-^{11}C]-methionine in human glioma cell lines. *Brain Res.* 2013;1535:24–37.
45. Oka S, Okudaira H, Ono M, et al. Differences in transport mechanisms of trans-1-amino-3-[^{18}F]fluorocyclobutanecarboxylic acid in inflammation, prostate cancer, and glioma cells: comparison with l-[methyl-^{11}C]methionine and 2-deoxy-2-[^{18}F]fluoro-D-glucose. *Mol Imaging Biol.* 2014;16:322–329.
46. Scarpelli ML, Healey DR, Mehta S, Quarles CC. Imaging glioblastoma with ^{18}F-fluciclovine amino acid positron emission tomography. *Front Oncol.* 2022;12:829050.
47. Verger A, Filss CP, Lohmann P, et al. Comparison of O-(2-^{18}F-fluoroethyl)-L-tyrosine positron emission tomography and perfusion-weighted magnetic resonance imaging in the diagnosis of patients with progressive and recurrent glioma: a hybrid positron emission tomography/magnetic resonance study. *World Neurosurg.* 2018;113:e727–e737.
48. Jena A, Taneja S, Gambhir A, et al. Glioma recurrence versus radiation necrosis: single-session multiparametric approach using simultaneous O-(2-^{18}F-fluoroethyl)-L-tyrosine PET/MRI. *Clin Nucl Med.* 2016;41:e228–e236.
49. Steidl E, Langen KJ, Hmeidan SA, et al. Sequential implementation of DSC-MR perfusion and dynamic [^{18}F]FET PET allows efficient differentiation of glioma progression from treatment-related changes. *Eur J Nucl Med Mol Imaging.* 2021;48:1956–1965.
50. Werner JM, Stoffels G, Lichtenstein T, et al. Differentiation of treatment-related changes from tumour progression: a direct comparison between dynamic FET PET and ADC values obtained from DWI MRI. *Eur J Nucl Med Mol Imaging.* 2019;46:1889–1901.
51. Turkbey B, Mena E, Shih J, et al. Localized prostate cancer detection with ^{18}F FACBC PET/CT: comparison with MR imaging and histopathologic analysis. *Radiology.* 2014;270:849–856.